Author Manuscript

Author Manuscript

Author Manuscript

Author Manuscript

HHS Public Access

Author manuscript

Neuroimage. Author manuscript; available in PMC 2018 February 01.

Published in final edited form as:

Neuroimage. 2017 February 01; 146: 701–714. doi:10.1016/j.neuroimage.2016.10.019.

A framework for designing dynamic lp-ntPET studies to maximize the sensitivity to transient neurotransmitter responses to drugs: application to dopamine and smoking

Shuo Wang[a,b], **Sujin Kim**[a,c], **Kelly P. Cosgrove**[a,c,d], and **Evan D. Morris**[*,a,b,c,d]

[a]Yale PET Center, Yale University, New Haven, Connecticut, USA

[b]Department of Biomedical Engineering, Yale University, New Haven, Connecticut, USA

[c]Department of Radiology and Biomedical Imaging, Yale University, New Haven, Connecticut, USA

[d]Department of Psychiatry, Yale University, New Haven, Connecticut, USA

Abstract

The “linear parametric neurotransmitter PET” (lp-ntPET) model was introduced to capture the time course of transient endogenous neurotransmitter response to drug stimulus from dynamic PET data. We previously used this novel analysis tool to probe the short-lived dopamine (DA) response induced by cigarette smoking in the PET scanner. It allowed us to find a sex difference in the DA signature of cigarette smoking. To make best use of this tool to characterize neurotransmitter response to drug stimulus, the sensitivity of lp-ntPET to detect such responses must be maximized. We designed a series of simulation studies to examine the impact of the following factors on the sensitivity of lp-ntPET using smoking-induced DA release as an example application: tracer delivery protocol, pre-processing for image denoising, timing of the smoking task, duration of the PET scan, and dose of the radiotracer. Our results suggest that a Bolus paradigm could replace a more difficult B/I paradigm without sacrificing the sensitivity of the method. Pre-processing the PET data with the de-noising algorithm HYPR could improve the sensitivity. The optimal timing to start the smoking task is 45min in a 90min scan and 35min in a 75min scan. A mild shortening of the scan time from 90mCi to 75min should be acceptable without loss of sensitivity. We suggest a lower dose limit of a bolus injection at 16mCi to limit underestimation of DA activation. This study established the framework to optimize the experimental design for reaching the full potential of lp-ntPET to detect neurotransmitter responses to drugs or even behavioral tasks.

Graphical Abstract

[*]**Corresponding Author:** Dr. Evan D. Morris, Yale PET Center, 801 Howard Avenue, New Haven, CT 06520, USA. Tel: 1-203-737-5752. evan.morris@yale.edu.

Publisher's Disclaimer: This is a PDF file of an unedited manuscript that has been accepted for publication. As a service to our customers we are providing this early version of the manuscript. The manuscript will undergo copyediting, typesetting, and review of the resulting proof before it is published in its final citable form. Please note that during the production process errors may be discovered which could affect the content, and all legal disclaimers that apply to the journal pertain.

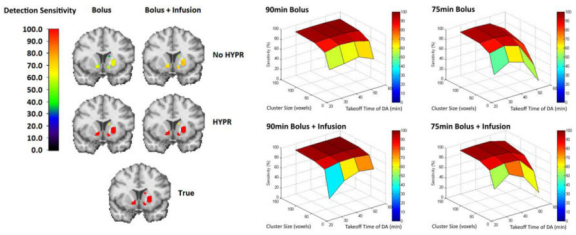

Keywords

PET; voxel analysis; neurotransmitter; dopamine; drug; smoking

1. Introduction

The “linear parametric neurotransmitter PET” (lp-ntPET) method was introduced (Normandin et al., 2012; Kim et al., 2014) to characterize the temporal patterns of time-varying neurotransmitter release induced by drug stimulus from dynamic PET data. We used this novel analysis tool previously to estimate DA response to cigarette smoking in the PET scanner. It allowed us to identify a sex difference in the brain’s DA signature of cigarette smoking (Cosgrove, Wang et al., 2014). We found that nicotine-dependent men responded rapidly and consistently to cigarette smoking in the right ventral striatum, the locus of the reinforcement effect of drugs such as nicotine. Women did not. A secondary finding was that, women responded faster than men in a part of the dorsal putamen, which has been implicated in habit formation (Porrino et al., 2004; Everitt and Robbins, 2013). These findings are consistent with the established notions that men smoke primarily for the reinforcing drug effect of nicotine (Perkins et al., 2001), while women tend to smoke cigarettes for other reasons, such as to alleviate stress and negative mood or out of habit.

None of the temporal differences that we observed could have been discovered without lp-ntPET. To make best use of this novel analysis tool to characterize neurotransmitter response to stimulus, the sensitivity of lp-ntPET to detect such responses must be maximized. We experienced several challenges that may have weakened the power of lp-ntPET. One obstacle was getting sufficient radioactivity dose. In our smoking study, our tracer delivery protocol was set to deliver 20mCi of [^{11}C]raclopride in a 90min bolus plus constant infusion scan with a K_{bol} of 105 min. It is quite a demanding burden on us to produce sufficient radioactivity following this protocol. Lower radioactivity dose could lead to greater noise and lower sensitivity of our method. Another challenge was the high noise level of voxel-by-voxel analysis. We believe lower noise in the voxel-level time activity curves (TACs) from the PET data will lead to more reliable parameter estimation. In addition, to better inform the neuroimaging community of the use of lp-ntPET, two remaining design parameters are the timing of the task and the duration of the scan.

Our goal in this study was to address these challenges by optimizing the experimental design and image processing procedure to achieve maximum sensitivity of lp-ntPET in detecting transient neurotransmitter response induced by stimulus. To this end, we designed a series of simulation studies to assess the impact of the following factors on the sensitivity of lp-

Author Manuscript Author Manuscript Author Manuscript Author Manuscript

Author Manuscript Author Manuscript Author Manuscript Author Manuscript

ntPET: 1. tracer delivery protocol, 2. pre-processing for image denoising, 3. timing of the challenge/task, 4. duration of the PET scan, and 5. dose of the radiotracer.

Among many possible applications, one application of lp-ntPET is to probe the short-lived DA response to cigarette smoking. Smoking remains the leading preventable cause of death in the US. Quitting smoking is extremely hard and current therapies to aid in smoking cessation are not effective enough. The primary addictive chemical in tobacco is nicotine. Nicotine, along with most drugs of abuse, has been shown to cause DA release (Di Chiara and Imperato 1988). Dopamine has been critically implicated in the reinforcing effects of nicotine and tobacco cigarette smoking. A number of PET imaging studies attempted to measure smoking-induced striatal DA release (Barrett et al., 2004; Brody et al., 2004, 2006; Scott et al., 2007), but with highly variable results. We believe these inconsistencies observed were due to reliance on conventional PET methods that were really only appropriate to detect sustained DA release (Sullivan et al., 2013) (e.g., in response to amphetamine administration). But, the DA response to cigarette smoking is brief (lasting only minutes).

In addition, it has been suggested that a drug's addictive liability may be dependent on the timing of DA release (Volkow et al., 2003), something that cannot be assessed in humans with conventional PET analysis methods. To probe the short-lived neurotransmitter response to drug stimulus in PET data on a voxel-by-voxel basis, we developed lp-ntPET (Morris et al., 2005, 2008, 2013; Normandin et al., 2008, 2012; Kim et al., 2014). This method allows us to characterize the important temporal patterns of transient DA release with parametric images of DA parameters and "DA movies" (Morris et al., 2013) of the brain from [^{11}C]raclopride PET scans. The strength of lp-ntPET over conventional methods has two main parts. One, it is designed to detect short-lived time-varying neurotransmitter response, and is thus ideal for imaging the DA response to cigarette smoking. Two, the resulting parametric images contain timing information about DA activation that was not previously measurable *in vivo*.

By optimizing the experimental design and image processing procedure to maximize the sensitivity of the lp-ntPET method to detect short-lived neurotransmitter response, we found in our simulation studies: 1. a tracer delivery protocol that saves radioactivity, 2. a pre-processing algorithm that reduces noise, 3. an optimal timing of the task that yields maximum sensitivity, 4. a shorter scan duration that preserve performance, and 5. a minimum dose of the radiotracer to maintain a consistently high sensitivity. The application of lp-ntPET is not limited to imaging DA release or cigarette smoking. This study established the framework to optimize the experimental design for use with lp-ntPET analysis in a broader field of neuroimaging research to detect neurotransmitter responses to drugs or even behavioral tasks.

Materials and Methods

2.1 Lp-ntPET Model

Eq. (1) shows the operational equation of lp-ntPET (Normandin et al., 2012). The first three terms are the MRTM model (Ichise et al., 2003) that considers endogenous DA to be time-

Author Manuscript Author Manuscript Author Manuscript Author Manuscript

invariant. The additional term (dashed in Eq. (1)) describes the pattern of transient DA release induced by smoking/drug challenge by extending the LSRRM of Alpert et al. (2003) using a basis function approach.

$$C_T(t) = R_1 C_R(t) + k_2 \int_0^t C_R(u)du - k_{2a} \int_0^t C_T(u)du - \gamma \int_0^t C_T(u) h_i(u) du \quad (1)$$

C_T and C_R are the concentrations in the target and reference region, respectively. R_1 is delivery ratio, k_2 is a transfer rate constant between the free compartment and the plasma, and k_{2a} is the apparent transfer rate constant between the target tissue (taken as one compartment) and the plasma. $h_i(t)$ is one of the possible response functions in a predefined library. The coefficient γ is the magnitude of the time varying response $h_i(t)$.

The library of possible response functions includes gamma-variate functions [Eq. (2a)] and pure exponential functions [Eq. (2b)].

$$h_i(t) = \left(\frac{t - t_D}{t_P - t_D}\right)^{\alpha} \exp\left(\alpha\left[1 - \frac{t - t_D}{t_P - t_D}\right]\right) u(t - t_D) \quad (2a)$$

$$h_i(t) = \exp(\beta(t - t_D)) u(t - t_D) \quad (2b)$$

The variable t_D is a response start time (relative to the start of the tracer), t_P is a peak response time (relative to the start of the tracer), α represents sharpness of the function, and β is the exponential time constant. During the curve fitting process, only one of the response functions from the library is used for a given fit. The response function with the best fit is chosen.

The lp-ntPET model is applied voxel-by-voxel to all the PET data. Using an F test, at each voxel the fit with lp-ntPET is compared to the fit with MRTM. This generates an F statistics map as a measure of the improvement of the fit achieved by lp-ntPET over MRTM, corrected by degrees of freedom. The F statistics map is first thresholded by an F statistics value that translates to a p-value<0.05 and then thresholded by a cluster size threshold to correct for multiple comparisons and controls the false positive rate<10%. The remaining voxels after the thresholding processes are identified to contain significant DA release. The details of the theory and implementation of lp-ntPET have been described by Kim et al. (2014).

2.2 Simulations

Noisy and noiseless striatal [^{11}C]raclopride time activity curves (TACs) with DA release at various time points were simulated for scan durations of 90 and 75 min in 3-min frames. To

Author Manuscript Author Manuscript Author Manuscript Author Manuscript

best represent the real data, our simulated noisy data used a similar noise level as was found in voxel-level TACs from a real human [^{11}C]raclopride scan. The noiseless TACs were simulated using the full 'ntPET' model (Morris et al., 2005), which is a nonlinear model of tracer binding to a receptor in the presence of a time-varying endogenous competitor. The simulations were implemented in Matlab (R2012b, MathWorks, Inc., Natick, MA) using modeling functions provided by a library of COMKAT (Muzic and Cornelius, 2001).

2.2.1 Input Function—Different input functions were used for simulating different injection protocols. **1. Input function for simulating bolus data.** The simulated Bolus data used an input function (Figure 1a) taken from [^{11}C]raclopride rest scan following a Bolus injection of 20mCi into a male subject (85.45 kg). The simulation of 90 min and 75 min data used the first 90 min or 75 min of the input function, as needed. The simulation of Bolus data with varied delivered doses used the above input function scaled by dose (scale factor = delivered dose/20mCi). **2. Input function for simulating bolus plus constant infusion data.** The input function following a bolus plus constant infusion (B/I) protocol (Figure 1b) with a K_{bol}=105min, a scan duration T=90min and delivered dose of 20mCi (equivalent to a dose of 29.36 mCi at the beginning of the scan) was calculated using the Equation (3) (Carson et al., 1993),

$$g(t)=\frac{K_{\mathrm{bol}}f(t)+\int_0^t f(\tau)d\tau}{K_{\mathrm{bol}}+T} \quad (3)$$

where $g(t)$ is the predicted input function following a B/I protocol, and $f(t)$ is the input function following a bolus administration of 29.36 mCi of [^{11}C]raclopride. The input function following a B/I protocol with Kbol=105 min, T=75 min and delivered dose of 20 mCi (equivalent to a dose of 27.29 mCi at the beginning of the scan) was calculated using the same equation with $f(t)$ being the input function following a bolus administration of 27.29 mCi of [^{11}C]raclopride. Because the total delivery is over a shorter period of time, there is less decay during infusion and less dose is required at start.

2.2.2 Kinetic Parameters—Kinetic parameters were set for the target region (striatum) and the reference region (cerebellum) based on typical parameters values stated in Pappata et al., 2002. **1. Kinetic parameters for target region.** For all simulations, the striatal kinetic parameters were set as K_1=0.07344 mL/(min g), k_2=0.35872 min^{-1}, k_{on}=0.0173 mL/(pmol min), k_{off}=0.1363 min^{-1}, B_{max}=44 pmol/mL, and F_v= 0.04 mL/mL. **2. Kinetic parameters for reference region.** A noiseless cerebellum TAC was also simulated for each study paradigm as the reference region TAC using the same model by setting K_1=0.0918 mL/(min g), k_2=0.4484 min^{-1}, and k_{on}^{DA}=k_{off}^{DA}=0.

2.2.3 DA Parameters—Free endogenous DA (F^{DA}) was modeled as a gamma-variate function plus a constant baseline [Eq. (4)], with the start of DA release, t_D, the peak time of DA, t_P, the sharpness, α, and the peak DA level, γ. The F^{DA} function was applied to the full ntPET model. The DA binding parameters (association and dissociation rates) were set as k_{on}^{DA}=0.25 mL/(pmol min) and k_{off}^{DA}=25 min^{-1} (Morris et al., 1995). **1. DA parameters**

Author Manuscript Author Manuscript Author Manuscript Author Manuscript

for null data. To simulate null data, the basal DA level was set as 100 nM, and the peak DA level = 0 (no DA elevation above the basal DA level) (Figure 2a). **2. DA parameters for smoking data.** To simulate smoking data, the basal DA level was set as 100 nM, and the peak DA level = 200 nM above basal level (Figure 2b). A series of timing parameters were applied to the gamma-variate function to simulate varied start time of cigarette smoking during the scan with takeoff time t_D=[25, 35, 45, 55]min, peak time t_P= t_D+10 min, and sharpness α=1.

$$F^{DA}(t)=\text{basal } DA+\gamma\left(\frac{t-t_D}{t_P-t_D}\right)^{\alpha} exp\left(\alpha\left[1-\frac{t-t_D}{t_P-t_D}\right]\right) u(t-t_D) \quad (4)$$

2.2.4 Noise—Gaussian noise was added to the noiseless target tissue TACs (Figure 2c, 2d, 2g, 2h) with zero mean and the following standard deviation corresponding to the *i*th time frame [Eq. (5)](Kim et al., 2014).

$$\sigma=\mu\times\left(\sqrt{(C_T(t_i)\times e^{-\lambda t_i})/\Delta t_i}\right)\times e^{\lambda t_i} \quad (5)$$

The scale factor μ determines the noise level, $C_T(t_i)$ is the target tissue tracer concentration of the *i*th frame in the simulated noiseless TAC, λ is the decay constant for Carbon-11, and Δt_i is the frame length of the *i*th time frame. To reflect the noise level in the real data, the scale factor μ was set at 0.8 to achieve the same mean coefficient of variation as that in a 90-min B/I [^{11}C]raclopride PET rest scan acquired in the HRRT PET scanner (Siemens/CTI, Knoxville, TN) in a human subject with a 20mCi delivered radioactivity. The voxel-level coefficient of variation in the real data was determined from the ratio of the standard deviation to the mean of the last 15 min of [^{11}C]raclopride PET concentration in each individual voxel within the ventral-striatum region. Then the mean coefficient of variation was calculated by fitting a Gaussian to the voxel-level coefficient of variation in all voxels. To validate that the noise level in the simulated noisy data (Figure 2e, 2f, 2i, 2j) was similar to that in the real data, the distributions of F statistics (Figure 3) after applying lp-ntPET were compared between the two datasets following procedures described in Kim et al., 2014.

2.3 Creating a 4D Phantom

To create a 4D phantom, simulated noisy TACs were placed into a 3D striatal template which contains 4 coronal slices and 1004 voxels in the MNI template space corresponding to the precommissural striatum (ventral striatum, dorsal caudate, and dorsal putamen) (Martinez et al., 2003). **1. Null phantom.** To create a single 4D null phantom, 1004 noisy TACs of null data were simulated and assigned to each of the 1004 voxels in our striatal template (Figure 4a). For each injection protocol, 100 null phantoms were created. **2. Smoking phantom.** To create a smoking phantom, 4 clusters (Figure 4b) of different sizes: [16, 32, 64, 128] voxels within the striatal template were filled with noisy TACs of smoking data, while the remaining voxels (Figure 4c) in the template were filled with noisy TACs of null data. Clusters were 3D. They existed in all 4 slices of the 3D striatal template. Thus we

Author Manuscript Author Manuscript Author Manuscript Author Manuscript

simulated 4 local volume of activation within the striatal volume of interest. For each smoking study paradigm, 100 smoking phantoms were generated.

2.4 HYPR De-noising

The simulated 4D phantoms were first processed by "HighlY constrained backPRojection" (HYPR) (Christian et al., 2010). The HYPR processing is an image de-noising algorithm that reduces noise in the PET TACs while preserving critical temporal patterns in the data. The algorithm was implemented in this study using a 3 × 3 × 3 voxels 3D boxcar smoothing filter, and the entire time series of data as the composite image.

2.5 Modeling

The lp-ntPET model was applied to fit the PET data voxel-by-voxel in all phantoms we created (pre and post HYPR de-noising). The MRTM model was also applied to fit the same data. The weighted residual sum of squares (WRSS) of both fits in all voxels were recorded. For lp-ntPET fits, we used the following discrete set of parameter values for the gamma-variate response function for characterizing patterns of DA response induced by smoking a cigarette. The sharpness parameter α were set to include 3 possible values: 0.25, 1, and 4. Response start times (t_D) were set between (smoking time - 5 min) to (smoking time + 15 min) in increments of 1.5 min. Peak response times (t_P) were set between (t_D + 1.5 min) and (total scan time - 5 min) in increments of 1.5 min. (Kim et al., 2014)

2.6 F-test Thresholding

An F statistics map (Figure 5a, 6a) was generated with the F statistics calculated [Eq. (6)] (Kim et al., 2014) for each voxel in the phantom, where $WRSS_i$ and p_i are the WRSS and number of parameters, respectively, for model i, and n is the number of data points in a PET TAC. The F statistics, in this case, is a measure of the improvement of the fit achieved by lp-ntPET over MRTM, corrected by degrees of freedom. The F statistics map was thresholded by the F statistics value that translates to a p-value<0.05. This step generated the Preliminary Significance Mask (Figure 5b, 6b) which was a binarized mask in which 1 represents presence of significant DA release in a given voxel.

$$F=\frac{\left(\frac{\mathrm{WRSS}_{\mathrm{MRTM}}-\mathrm{WRSS}_{\mathrm{lp-ntPET}}}{p_{\mathrm{lp-ntPET}}-p_{\mathrm{MRTM}}}\right)}{\left(\frac{\mathrm{WRSS}_{\mathrm{lp-ntPET}}}{n-p_{\mathrm{lp-ntPET}}}\right)} \quad (6)$$

2.7 Cluster-size Thresholding

To correct for multiple comparisons, a cluster-size threshold was applied to the Preliminary Significance Mask to generate the Final Significance Mask (Figure 5c, 6c). The cluster-size threshold was determined for each study protocol from simulated null data (Kim et al., 2014). For each protocol, the 100 simulated noisy null phantoms were processed, yielding 100 Preliminary Significance Masks containing clusters of various sizes that were identified as containing significant DA release in the null data, and were therefore false positive clusters. A first-pass cluster size threshold was determined so that 99% (Figure 5d) of the

Author Manuscript Author Manuscript Author Manuscript Author Manuscript

total false positive clusters in the 100 significance maps were eliminated. The cluster size threshold was further adjusted to ensure that 90 out of 100 null phantoms were completely free of false positive clusters (Figure 5e).

2.8 Metrics for Comparing Detection Sensitivities

For each protocol, the 100 simulated noisy smoking phantoms were processed, with corresponding cluster size threshold applied, yielding 100 Final Significance Masks (Figure 6d) containing clusters that were identified to contain significant DA release in the smoking data. We have defined sensitivity in two ways to fully characterize the performance of our method.

2.8.1 The Mean Voxel-by-Voxel Sensitivity—The 100 binary final significance masks (Figure 6d) were summed (Figure 6e) and filtered by the binary template of true clusters of activation (Figure 6f) to generate a sensitivity map (Figure 6g). Each voxel in the sensitivity map contains a sensitivity value ranging from 0 to 100 representing the number of smoking phantoms out of 100 phantoms in which DA activation was detected at a given voxel. The Mean Voxel-by-Voxel (MV) Sensitivity was calculated as the mean of the voxel-by-voxel sensitivity values across all voxels containing a true cluster of activation [Eq. (7)] (Figure 7). By rearrangement, the MV Sensitivity can be interpreted as the Mean Percent of Spatial Extent in the region containing true DA activation that is detected, averaged over 100 simulations [Eq. (8)].

$$\text{Mean Sensitivity}=\frac{\sum_{i=1}^{N_{\text{Voxels}}}\frac{1}{100}\text{sensitivity}_{\text{Voxel } i}}{N_{\text{Voxels}}}=\frac{\sum_{i=1}^{N_{\text{Voxels}}}\frac{1}{100}\left(\sum_{j=1}^{100}I_{\text{Voxel } i,\text{Phantom } j}\right)}{N_{\text{Voxels}}} \quad (7)$$

$$\begin{aligned}\text{Mean Sensitivity}&=\frac{\frac{1}{100}\sum_{j=1}^{100}\left(\sum_{i=1}^{N_{\text{Voxels}}}I_{\text{Voxel } i,\text{Phantom } j}\right)}{N_{\text{Voxels}}}\\&=\frac{1}{100}\sum_{j=1}^{100}\frac{\sum_{i=1}^{N_{\text{Voxels}}}I_{\text{Voxel } i,\text{Phantom } j}}{N_{\text{Voxels}}}\\&=\frac{1}{100}\sum_{j=1}^{100}\text{Percent of Spatial Extent}_{\text{Phantom } j}=\text{Mean Percent of Spatial Extent}\end{aligned} \quad (8)$$

N_{Voxels} is the number of voxels in a true cluster of activation, $Sensitivity_{Voxel\ i}$ represents the number of smoking phantoms out of 100 phantoms in which DA activation was detected at the i_{th} voxel, and $I_{Voxel\ i,Phantom\ j}$ is the binary value with 1 representing ‘activation’ detected and 0 representing ‘no activation’ detected at the i_{th} voxel in the j_{th} simulated smoking phantom.

Author Manuscript Author Manuscript Author Manuscript Author Manuscript

2.8.2 Binary Cluster Detection Sensitivity—The Binary Cluster Detection (BC) Sensitivity was calculated as the number of simulated phantoms with final significance masks that partially overlapped with the mask of clusters in the true phantom (Figure 8). This definition asked the "yes" or "no" question: was a given cluster of activation detected in a simulated phantom. The answer was "yes" when as long as part of the cluster in the true phantom was identified to contain DA release in the simulated phantom. The BC Sensitivity counted the number of simulated phantoms that were positively detected out of 100 simulated phantoms and thus represents the percent chance of a true DA activation being detected without regard to a perfect recovery of all voxels in the cluster.

2.9 Study Design

We designed 5 different simulation studies to address 5 impacting factors on the sensitivity of lp-ntPET. **Study 1. Tracer Delivery.** A Bolus and a B/I dataset were simulated and analyzed to compare the sensitivity of lp-ntPET in detecting transient DA release between these two practices of tracer delivery. The Bolus paradigm was simulated as a Bolus injection of 20mCi of [^{11}C]raclopride with a 90min scan duration. The B/I paradigm was simulated with a 90min scan duration, a K_{bol} of 105min and total delivered dose of 20mCi. In both studies, the smoking-induced DA release was simulated to take off at 35min after the beginning of the injection. **Study 2. Pre-processing.** The Bolus and B/I datasets in Study 1 were each processed twice following two different procedures to assess the impact of HYPR de-noising on the sensitivity of lp-ntPET in detecting transient DA release. In one case, there was no pre-processing before fitting data with the lp-ntPET model. In the second case, phantom data were pre-processed with the HYPR de-noising algorithm prior to data fitting. In our implementation of HYPR, we used a (3 × 3 × 3 voxels) 3D boxcar smoothing filter, and a time-averaged composite image generated from the entire time series of data. **Study 3. Optimal Timing of Task.** A series of Bolus (Figure 9b) and B/I (Figure 9c) datasets were simulated to include DA activation starting at one of four different time points during the scan to determine the optimal timing to start the smoking task. The DA activations were simulated as gamma variate functions with take off time t_D=[25, 35, 45, 55]min. Peak time was determined, accordingly, as $t_P=t_D$+10min (Figure 9a). **Study 4. Scan Duration.** Another series of datasets were simulated to include DA activation with all the same DA parameters as in Study 3, but with only a 75min scan duration. **Study 5. Minimum Radioactivity Dose.** A series of Bolus studies were simulated to represent Bolus injections of 10mCi, 12mCi, 14mCi, 16mCi, 18mCi and 20mCi of [^{11}C]raclopride with a 75min scan duration (Figure 9d) to determine the minimum Bolus dose that would provide acceptable sensitivity.

3.Results

3.1 Tracer Delivery

The sensitivities of lp-ntPET in detecting the simulated DA release in the Bolus vs. B/I study without HYPR processing are shown in Figure 10 (green lines). With the same delivered radioactivity dose, the Bolus paradigm yielded lower MV Sensitivity vs. the B/I paradigm in all 4 simulated clusters containing DA release (green lines in Figure 10 a vs. b). The BC Sensitivity (green lines in Figure 10 c vs. d, Supplementary Table S1) were the same in the 3

Author Manuscript Author Manuscript Author Manuscript Author Manuscript

largest clusters for Bolus and B/I: 100% for the 64-voxel and 128-voxel clusters, and 99% for the 32-voxel cluster. In the smallest cluster (16 voxels), the BC Sensitivity for a Bolus study was lower than a B/I study (53% vs. 71%).

3.2 Pre-processing

The sensitivities in both Bolus and B/I studies when the data are pre-processed by the HYPR de-noising algorithm are shown by the orange lines in Figure 10. HYPR processing dramatically improved the MV Sensitivity in both paradigms (Figure 10 orange lines vs. green lines, Figure 11 bottom row vs. top row). In the Bolus paradigm, HYPR increased the MV Sensitivity from 32.2% to 60.0% (Figure 10a) in the smallest cluster containing 16 voxels with true DA activation, and from 62.2% to 98.8% in the biggest cluster (128 voxels). In the B/I paradigm, HYPR improved the MV Sensitivity from 49.5% to 62.9% (Figure 10b) in the smallest cluster (16 voxels), and from 71.6% to 99.2% in the biggest cluster (128 voxels). When the data in both paradigms were pre-processed by HYPR, the Bolus paradigm yielded similar MV Sensitivity as the B/I (orange lines in Figure 10 a vs. b), and almost identical BC Sensitivity as the B/I (orange lines in Figure 10 c vs. d, Supplementary Table S2).

3.3 Optimal Timing of Task

Tables I–IV presents the influence of different takeoff times of simulated DA activation (as a representation of the start time of a smoking task) on the sensitivity in 90min Bolus and B/I studies. In the 90min Bolus paradigm, the MV Sensitivity was highest when DA started to rise from baseline at 35 or 45min following tracer injection (Figure 12a and Table I). The highest BC Sensitivity for the 16-voxel cluster was 77% for a DA curve that took off at 45min, 100% for the 32-voxel cluster when DA took off at 35, 45 or 55min, and 100% for clusters of 64 and 128 voxels regardless of DA takeoff times (Table II). In the 90min B/I paradigm, the maximum MV Sensitivity was achieved when DA took off at 45min (Figure 12b and Table III). The highest BC Sensitivity for the 16-voxel cluster was 84% when DA took off at 55min, 100% for the 32-voxel cluster when DA took off at 35, 45 or 55min, and 100% for the other 2 clusters regardless of DA takeoff times (Table IV).

3.4 Scan Duration

The sensitivity in 75min Bolus and B/I studies with different takeoff times for DA is shown in Tables V–VIII. In the 75min Bolus paradigm, the maximum MV Sensitivity was achieved when DA took off at 35min (Figure 12c and Table V). The highest BC Sensitivity for the 16-voxel cluster was 81% for a DA curve that took off at 35min, 100% for the 32-voxel cluster when DA took off at 35min or 45min, and 100% for the 64-voxel and 128-voxel clusters regardless of DA takeoff times (Table VI). In the 75min B/I paradigm, the maximum MV Sensitivity occurred when DA took off at 35min (Figure 12d and Table VII). The highest BC Sensitivity for the 16-voxel cluster was 86% when DA took off at 35min, 100% for the 32-voxel cluster when DA took off at 25, 35 or 45min, and 100% for the 64-voxel and 128-voxel clusters regardless of DA takeoff times (Table VIII).

The comparison of 75min to 90min scan duration revealed that the highest MV Sensitivity and BC Sensitivity achieved in a 75min scan (Tables V–VIII) was as good as that in a 90min

Author Manuscript Author Manuscript Author Manuscript Author Manuscript

scan (Tables I–IV). The MV Sensitivity and BC Sensitivity for a DA curve that took off at 55min were much smaller for a 75min scan (last row in Tables V–VIII) as compared to a 90min scan (last row in Tables I–IV).

3.5 Minimum Radioactivity Dose

In 75min Bolus studies with different delivered radioactivity doses, the MV Sensitivity for activated clusters of all sizes gradually decreased as lower and lower delivered doses were simulated (Supplementary Table S3 and Figure S1a). The BC Sensitivity for the 16-voxel cluster was almost unchanged when the dose decreased from 20mCi to 16mCi (from 81% to 80%), but started to drop as the dose was lowered to 14mCi (76%), and was very low at 10mCi (55%) (Supplementary Table S4 and Figure S1b). For the 3 largest clusters, the BC Sensitivity was constantly 100% when the dose dropped from 20mCi to 10mCi.

3.6 Cluster Size Threshold

In order to maintain all the same false positive rate to be less than 10% in the overall method, the cluster size threshold was varied across different study paradigms. The cluster size threshold was similar for Bolus and B/I without HYPR pre-processing. HYPR increased the cluster size threshold for Bolus from 11 to 28 voxels, and for B/I from 12 to 36 voxels in smoking studies containing DA activation that took off at 35min with a 90min scan duration and 20mCi of delivered radioactivity. As an example to illustrate the number of clusters thresholded out after first- and second-pass, for the 90min B/I studies with HYPR applied in the 100 simulated null phantoms, the total number of false positive clusters was 2693, the first-pass threshold was set at 29 voxels so that only 26 (<1% of 2693) false positive clusters were retained, i.e. 99% of false positive clusters were eliminated. The surviving 26 false positive clusters were distributed among 22 of the 100 null phantoms. The second-pass threshold was increased to 36 voxels, so that only 9 out of the 100 phantoms contained 1 false positive cluster, thus satisfying our goal that <10% phantoms have any false positive cluster. As the start time of task went later into the scan, the cluster size threshold became smaller. For example, the cluster size thresholds for Bolus studies containing DA activation that took off at [25, 35, 45, 55]min were [31, 28, 23, 15]voxels. The 75min scan required a smaller cluster size threshold than a 90min scan (e.g., for a Bolus study containing DA activation that took off at 35min, the cluster size threshold was 17 voxels for a 75min scan duration as compared to 28 voxels for a 90min scan duration). As the Bolus tracer dose was lowered from 20mCi to 10mCi, the cluster size threshold was generally unchanged until the dose reached 10mCi (17 voxels for [20, 18, 16, 14, 12]mCi Bolus doses, and 18 voxels for 10mCi).

4.Discussion

4.1 Bolus as an Alternative of B/I

Our main finding was that a Bolus yielded equivalent sensitivity as a B/I paradigm with the same delivered radioactivity dose provided that HYPR was applied. This finding from simulations provides important guidance for experimental design of future lp-ntPET experiments on smoking or similar behavioral tasks, especially when radioactivity dose may be limited. For a B/I injection of [^{11}C]raclopride with a delivered dose=20mCi, a

Author Manuscript Author Manuscript Author Manuscript Author Manuscript

Kbol=105min and a scan duration of 90min, the required pre-scan dose must be at least 29.4mCi. When the radioactivity produced by the radiochemistry lab falls below 29.4mCi pre-scan, an alternative paradigm, a Bolus of 20mCi of [^{11}C]raclopride could be administered without sacrificing the sensitivity of the lp-ntPET method. This finding suggests that when a high enough pre-scan dose for the B/I paradigm can not be consistently produced, the Bolus paradigm should be considered as an acceptable alternate design.

4.2 Contribution of HYPR De-noising

We found that HYPR dramatically improved the MV Sensitivity for both paradigms and the BC Sensitivity in the Bolus paradigm. We attribute improved sensitivity with HYPR to the effect of noise reduction in the TACs. In fact, we have previously shown the power of HYPR in reducing noise in the TACs of [^{11}C]raclopride PET data on the voxel level (Wang et al., 2012). In addition to HYPR, we also evaluated the impact of simple spatial smoothing on detection sensitivity and temporal precision of the recovered response profile. The results (see Supplementary text, Figures S2–S4 and Table S5) support the selection of HYPR over simple spatial smoothing.

4.3 Optimal Timing of the Smoking Task

Our results comparing smoking challenges starting at different time points during the scan favor a 45min start in a 90min scan and 35min start in a 75min scan as the optimal timing. The lp-ntPET analysis achieved its maximum sensitivity at these time points especially for small areas of activation (e.g., the cluster of 16 voxels in the true phantom). In much bigger areas of activation, the success rate of lp-ntPET in detecting transient DA release was consistently high (99%–100% BC Sensitivity) and insensitive to start time of smoking.

4.4 Scan Duration

We found that the maximum sensitivity in a 75min scan was as good as that in a 90min scan. This suggests that the duration of a smoking PET scan can be shortened from 90min to 75min. The advantage of shortening the scan duration is probably based on the fact that TACs in a 75min scan are less noisy than those in a 90min scan with the same delivered radioactivity dose and can thus reduce false positive findings. It should be noted that the 75min scan showed lower sensitivity compared to a 90min scan if DA takeoff was late (e.g., 55min). This was probably because as DA took off later, less perturbation to the shape of TACs introduced by the DA release was captured in the scan data. The difference between fits with MRTM and lp-ntPET became less pronounced. This suggests that late start time of tasks should be avoided when using a shorter scan.

4.5 The Minimum Radioactivity Dose

Our results comparing different doses of the radiotracer suggest a practical minimum dose of 16mCi in the bolus paradigm. Although the mean percent of detected spatial extent (reflected by the MV Sensitivity) gradually decreased as the delivered dose was lowered, the overall chance of detecting an activated region (the BC Sensitivity) was unchanged when the dose decreased from 20mCi to 16mCi, but started to drop as the dose was lowered to 14mCi. Doses lower than 16mCi of bolus injection could lead to underestimation of DA activation.

Author Manuscript Author Manuscript Author Manuscript Author Manuscript

That is, actual DA release in subjects who received lower than 16mCi of [^{11}C]raclopride would be detected less frequently due to lower sensitivity of the method.

4.6 Cluster Size Threshold

The cluster size threshold was intentionally varied across different study paradigms. With these cluster size thresholds applied to their corresponding study paradigms, the false positive rate was maintained to be constant (<10%) in the overall method. Although the cluster size threshold was increased by HYPR for Bolus from 11 to 28 voxels, and for B/I from 12 to 36 voxels (in smoking studies containing DA activation that took off at 35min with a 90min scan duration and 20mCi of delivered radioactivity), the sensitivity was still higher when HYPR was applied. That is, even with a larger cluster size threshold, HYPR allowed us to achieve higher sensitivity. This was because HYPR added spatial correlation to the neighboring voxels of true clusters containing DA activation, which effectively enlarged the areas of activation.

4.7 Limitations and Possible Uses

Only one shape of the DA response function was used in our simulation study. The peak height of DA activation was simulated to be 200% above the basal level. This peak height was picked based on results from previous microdialysis studies, which showed that administration of nicotine in doses equivalent to smoking produced 200% (Pontieri et al., 1996) and 250% (Domino and Tsukada, 2009) increases in extracellular DA above basal level in the striatum of rats and monkeys, respectively. In studies of cocaine and amphetamine, which were shown to be able to increase DA anywhere from 250 to 1,000% in the rat striatum (Carboni et al., 2001), the sensitivity of lp-ntPET to detect such DA activation with a lot greater magnitude would be much higher (Kim et al., 2014).

The timing of DA response in our simulations was assumed to take off as soon as the cigarette smoking started, and to rise to its peak height 10min after takeoff. This was typical of smoking one or two cigarettes based on estimated DA curves observed in our smoking study (Cosgrove, Wang et al., 2014). In our curve fitting process, the search space for the response start times (t_D) was bounded between (smoking time − 5 min) to (smoking time + 15 min). For PET experiments that involve drug challenges or behavioral tasks with different durations, the search space for response start times should be adjusted for the specific study. If the shape of the DA response induced by the drug/task is known to be different from the one we used, a tailored library of possible response functions specific to the drug/task should be constructed when implementing lp-ntPET.

The phantoms in this study were created by placing the simulated TACs into a 3D striatal template which contains 4 coronal slices and 1004 voxels in the MNI template space with a voxel size of $2 \times 2 \times 2$ mm^3. Since the phantoms were created and analyzed in the template space, the general conclusions in this study are not specific to our HRRT scanner. The absolute sensitivity values, though, are related to the noise level of the PET TACs which, in turn, depend on the characteristics of the PET scanner. For use with the HR+ scanner, which has lower spatial resolution (i.e., bigger voxel size) than the HRRT, the noise level of the TACs in individual voxels could be lower than our simulated noise level. The sensitivity of

Author Manuscript Author Manuscript Author Manuscript Author Manuscript

lp-ntPET to detect DA activation on the voxel level in less noisy PET data acquired by the HR+ scanner could be higher, but the chance of detecting small activated clusters could be lower due to the lower spatial resolution, i.e., if the activation locus is smaller than an HR+ voxel, then we'll miss the event entirely.

5. Conclusion

In this study, we optimized the design and pre-processing of PET studies using lp-ntPET analysis to detect short-lived DA release (such as we would expect from cigarette smoking) during a PET scan. Our simulations suggest that a Bolus paradigm could replace a more difficult B/I design and would not sacrifice the sensitivity of the method. The de-noising algorithm HYPR, in all circumstances, could improve the sensitivity of lp-ntPET. The optimal timing to start the smoking task is 45min in a 90min scan and 35min in a 75min scan. A mild shortening of the scan time from 90mCi to 75min should be acceptable without loss of sensitivity. We suggest setting the lower dose limit of a Bolus injection at 16mCi to limit possible underestimation of DA activation. Since the cluster size threshold to control the same false positive rate across different study paradigms must be varied, when designing a new lp-ntPET study, the cluster size threshold needs to be tailored for that specific study. We optimized the PET study design based on the shape of DA response that we believe applies to our smoking study. The general findings should apply to other studies that induce a similar DA response. If the shape of DA response induced by another challenge differs substantially from the one we used, additional simulations following the framework presented may be necessary.

Supplementary Material

Refer to Web version on PubMed Central for supplementary material.

Acknowledgments

The authors acknowledge the support of National Institute on Drug Abuse [R21DA032791, K02DA031750, and R01DA03870] and the Office of Research on Women's Health [P50DA033945].

References

Alpert NM, Badgaiyan RD, Livni E, Fischman AJ. A novel method for noninvasive detection of neuromodulatory changes in specific neurotransmitter systems. Neuroimage. 2003; 19:1049–1060. [PubMed: 12880831]

Barrett SP, Boileau I, Okker J, Pihl RO, Dagher A. The hedonic response to cigarette smoking is proportional to dopamine release in the human striatum as measured by positron emission tomography and [^{11}C]raclopride. Synapse. 2004; 54:65–71. [PubMed: 15352131]

Brody AL, Olmstead RE, London ED, Farahi J, Meyer JH, Grossman P, Lee GS, Huang J, Hahn EL, Mandelkern MA. Smoking-induced ventral striatum dopamine release. Am J Psychiatry. 2004; 161:1211–1218. [PubMed: 15229053]

Brody AL, Mandelkern MA, Olmstead RE, Scheibal D, Hahn E, Shiraga S, Zamora-Paja E, Farahi J, Saxena S, London ED, McCracken JT. Gene variants of brain dopamine pathways and smoking-induced dopamine release in the ventral caudate/nucleus accumbens. Arch Gen Psychiatry. 2006; 63:808–816. [PubMed: 16818870]

Author Manuscript Author Manuscript Author Manuscript Author Manuscript

Carboni E, Spielewoy C, Vacca C, Nosten-Bertrand M, Giros B, Di Chiara G. Cocaine and amphetamine increase extracellular dopamine in the nucleus accumbens of mice lacking the dopamine transporter gene. J Neurosci. 2001; 21:RC141, 1–4. [PubMed: 11312315]

Carson RE, Channing MA, Blasberg RG, Dunn BB, Cohen RM, Rice KC, Herscovitch P. Comparison of bolus and infusion methods for receptor quantitation: application to [^{18}F]Cyclofoxy and Positron Emission Tomography. J Cereb Blood Flow Metab. 1993; 13:24–42. [PubMed: 8380178]

Christian BT, Vandehey NT, Floberg JM, Mistretta CA. Dynamic PET denoising with HYPR processing. J Nucl Med. 2010; 51:1147–1154. [PubMed: 20554743]

Cosgrove KP, Wang S, Kim SJ, McGovern E, Nabulsi N, Gao H, Labaree D, Tagare HD, Sullivan JM, Morris ED. Sex differences in the brain's dopamine signature of cigarette smoking. J Neurosci. 2014; 34:16851–16855. [PubMed: 25505336]

Di Chiara G, Imperato A. Drugs abused by humans preferentially increase synaptic dopamine concentrations in the mesolimbic system of freely moving rats. Proc Natl Acad Sci USA. 1988; 85:5274–5278. [PubMed: 2899326]

Domino EF, Tsukada H. Nicotine sensitization of monkey striatal dopamine release. Eur J Pharmacol. 2009; 607:91–95. [PubMed: 19232339]

Everitt BJ, Robbins TW. From the ventral to the dorsal striatum: devolving views of their roles in drug addiction. Neurosci Biobehav Rev. 2013; 37:1946–1954. [PubMed: 23438892]

Ichise M, Liow JS, Lu JQ, Takano A, Model K, Toyama H, Suhara T, Suzuki K, Innis RB, Carson RE. Linearized reference tissue parametric imaging methods: application to [^{11}C]DASB positron emission tomography studies of the serotonin transporter in human brain. J Cereb Blood Flow Metab. 2003; 23:1096–1112. [PubMed: 12973026]

Kim SJ, Sullivan JM, Wang S, Cosgrove KP, Morris ED. Voxelwise lp-ntPET for detecting localized, transient dopamine release of unknown timing: Sensitivity analysis and application to cigarette smoking in the PET scanner. Hum Brain Mapp. 2014; 35:4876–4891. [PubMed: 24700424]

Martinez D, Slifstein M, Broft A, Mawlawi O, Hwang DR, Huang Y, Cooper T, Kegeles L, Zarahn E, Abi-Dargham A, Haber SN, Laruelle M. Imaging human mesolimbic dopamine transmission with positron emission tomography. Part II: amphetamine-induced dopamine release in the functional subdivisions of the striatum. J Cereb Blood Flow Metab. 2003; 23:285–300. [PubMed: 12621304]

Morris ED, Fisher RE, Alpert NM, Rauch SL, Fischman AJ. In vivo imaging of neuromodulation using positron emission tomography: Optimal ligand characteristics and task length for detection of activation. Hum Brain Mapp. 1995; 3:35–55.

Morris ED, Yoder KK, Wang C, Normandin MD, Zheng QH, Mock B, Muzic RF Jr, Froehlich JC. ntPET: a new application of PET imaging for characterizing the kinetics of endogenous neurotransmitter release. Mol Imaging. 2005; 4:473–489. [PubMed: 16285909]

Morris ED, Normandin MD, Schiffer WK. Initial comparison of ntPET with microdialysis measurements of methamphetamine-induced dopamine release in rats: Support for estimation of dopamine curves from PET data. Mol Imaging Biol. 2008; 10:67–73. [PubMed: 18176804]

Morris ED, Kim SJ, Sullivan JM, Wang S, Normandin MD, Constantinescu CC, Cosgrove KP. Creating dynamic images of short-lived dopamine fluctuations with lp-ntPET: dopamine movies of cigarette smoking. J Vis Exp. 2013; 78

Muzic RF Jr, Cornelius S. COMKAT: Compartment model kinetic analysis tool. J Nucl Med. 2001; 42:636–645. [PubMed: 11337554]

Normandin MD, Morris ED. Estimating neurotransmitter kinetics with ntPET: A simulation study of temporal precision and effects of biased data. Neuroimage. 2008; 39:1162–1179. [PubMed: 18023364]

Normandin MD, Schiffer WK, Morris ED. A linear model for estimation of neurotransmitter response profiles from dynamic PET data. Neuroimage. 2012; 59:2689–2699. [PubMed: 21767654]

Perkins KA, Gerlach D, Vender J, Grobe J, Meeker J, Hutchison S. Sex differences in the subjective and reinforcing effect of visual and olfactory cigarette smoke stimuli. Nicotine Tob Res. 2001; 3:141–150. [PubMed: 11403728]

Pontieri FE, Tanda G, Orzi F, Di Chiara G. Effects of nicotine on the nucleus accumbens and similarity to those of addictive drugs. Nature. 1996; 382:255–257. [PubMed: 8717040]

Author Manuscript Author Manuscript Author Manuscript Author Manuscript

Porrino LJ, Lyons D, Smith HR, Daunais JB, Nader MA. Cocaine self-administration produces a progressive involvement of limbic, association, and sensorimotor striatal domains. J Neurosci. 2004; 24:3554–3562. [PubMed: 15071103]

Scott DJ, Domino EF, Heitzeg MM, Koeppe RA, Ni L, Guthrie S, Zubieta JK. Smoking modulation of mu-opioid and dopamine D2 receptor-mediated neurotransmission in humans. Neuropsychopharmacology. 2007; 32:450–457. [PubMed: 17091130]

Sullivan JM, Kim S, Cosgrove KP, Morris ED. Limitations of SRTM, Logan graphical method, and equilibrium analysis for measuring transient dopamine release with [11C]raclopride PET. Am J Nucl Med Mol Imaging. 2013; 3:247–260. [PubMed: 23638336]

Volkow ND, Swanson JM. Variables that affect the clinical use and abuse of methylphenidate in the treatment of ADHD. Am J Psychiatry. 2003; 160:1909–1918. [PubMed: 14594733]

Wang S, Kim SJ, Sullivan JM, Gillard J, Gallezot JD, Cosgrove KP, Morris ED. Opitimization of HYPR filter for detection of smoking-Induced dopamine release in [^{11}C]Raclopride PET studies. J Cereb Blood Flow Metab. 2012; 32:S182.

Author Manuscript Author Manuscript Author Manuscript Author Manuscript

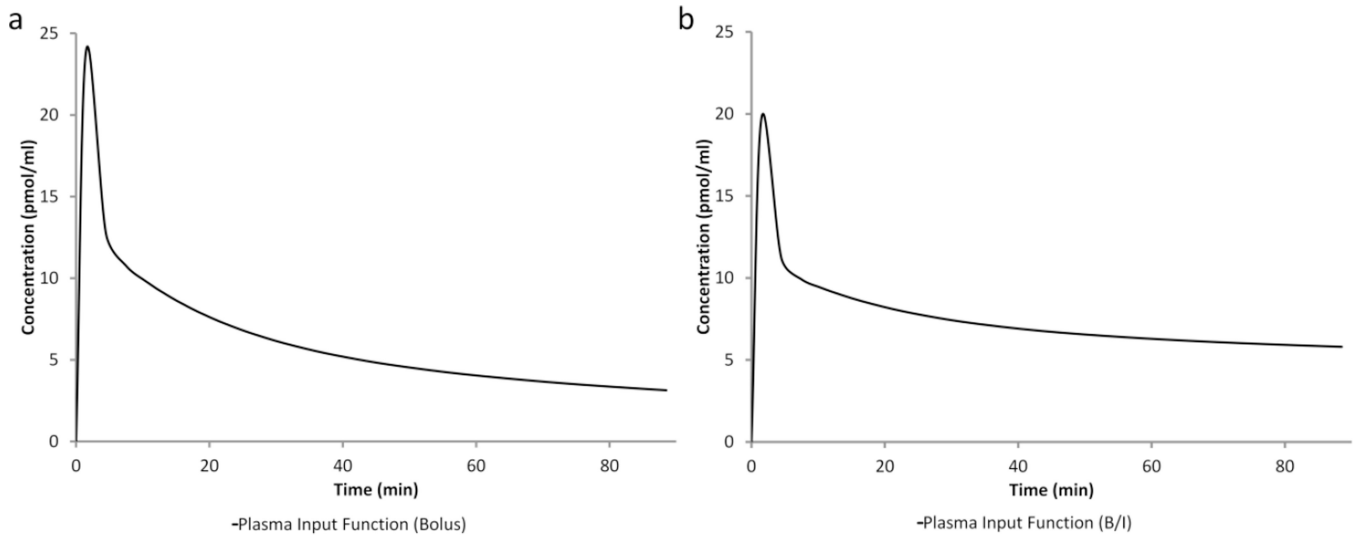

Figure 1.

a. Plasma input function for a Bolus injection of 20mCi. **b.** Plasma input function for a Bolus plus infusion (B/I) protocol with a K_{bol}=105 min, a scan duration T=90 min and total delivered dose of 20mCi.

Author Manuscript Author Manuscript Author Manuscript Author Manuscript

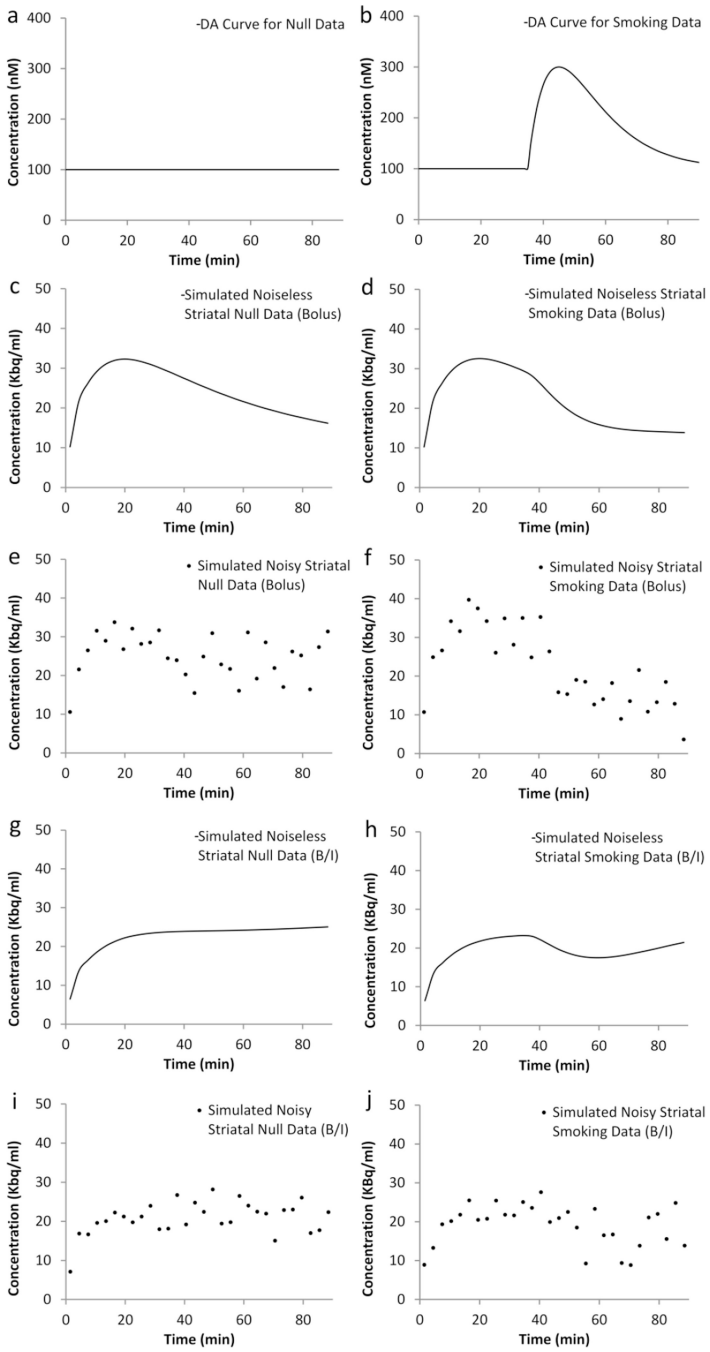

Figure 2.

a. Simulated DA curve for null data. **b.** An example of simulated DA curve for smoking data (DA takes off at 35min, peaks at 45min). **c.** Simulated noiseless striatal null data for a Bolus study. **d.** Simulated noiseless striatal smoking data for a Bolus study. **e.** Simulated noisy striatal null data for a Bolus study. **f.** Simulated noisy striatal smoking data for a Bolus study. **g.** Simulated noiseless striatal null data for a B/I study. **h.** Simulated noiseless striatal smoking data for a B/I study. **i.** Simulated noisy striatal null data for a B/I study. **j.** Simulated noisy striatal smoking data for a B/I study.

Author Manuscript Author Manuscript Author Manuscript Author Manuscript

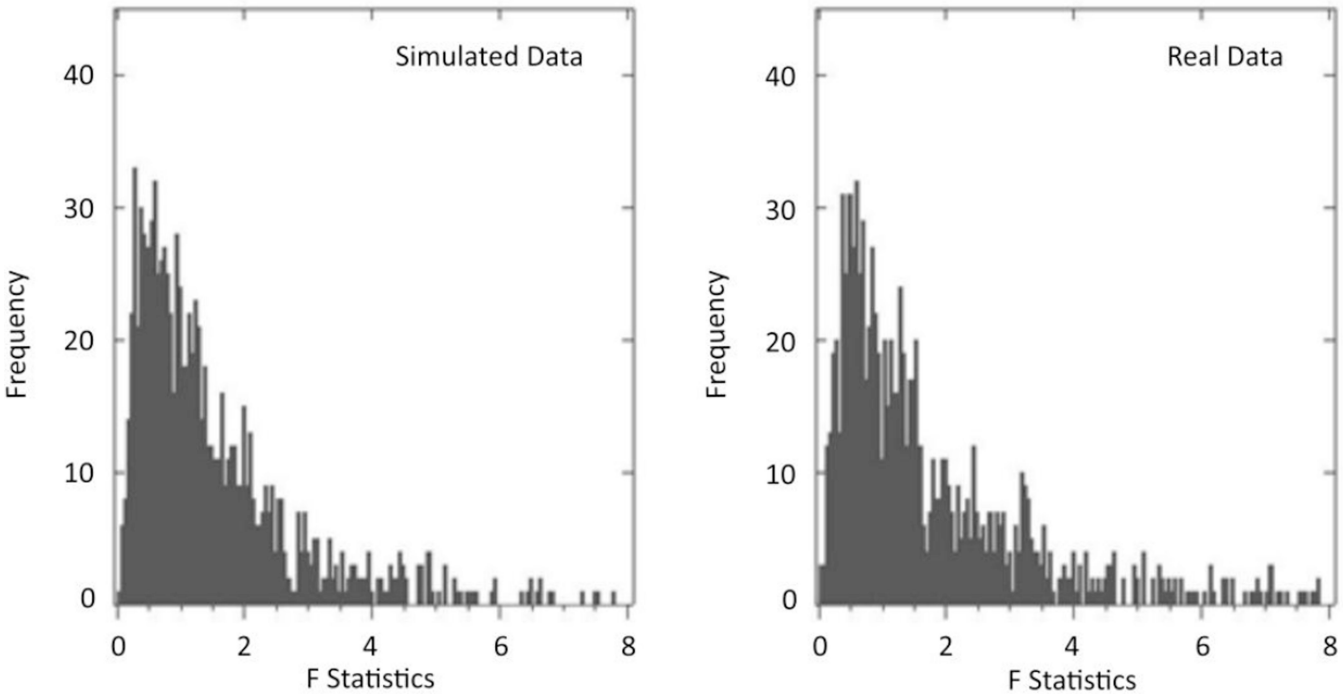

Figure 3.

Comparison of histograms of F statistics between simulated null data and real data from a rest scan. This comparison reflected similar noise level in the simulated data compared to the real data.

Author Manuscript Author Manuscript Author Manuscript Author Manuscript

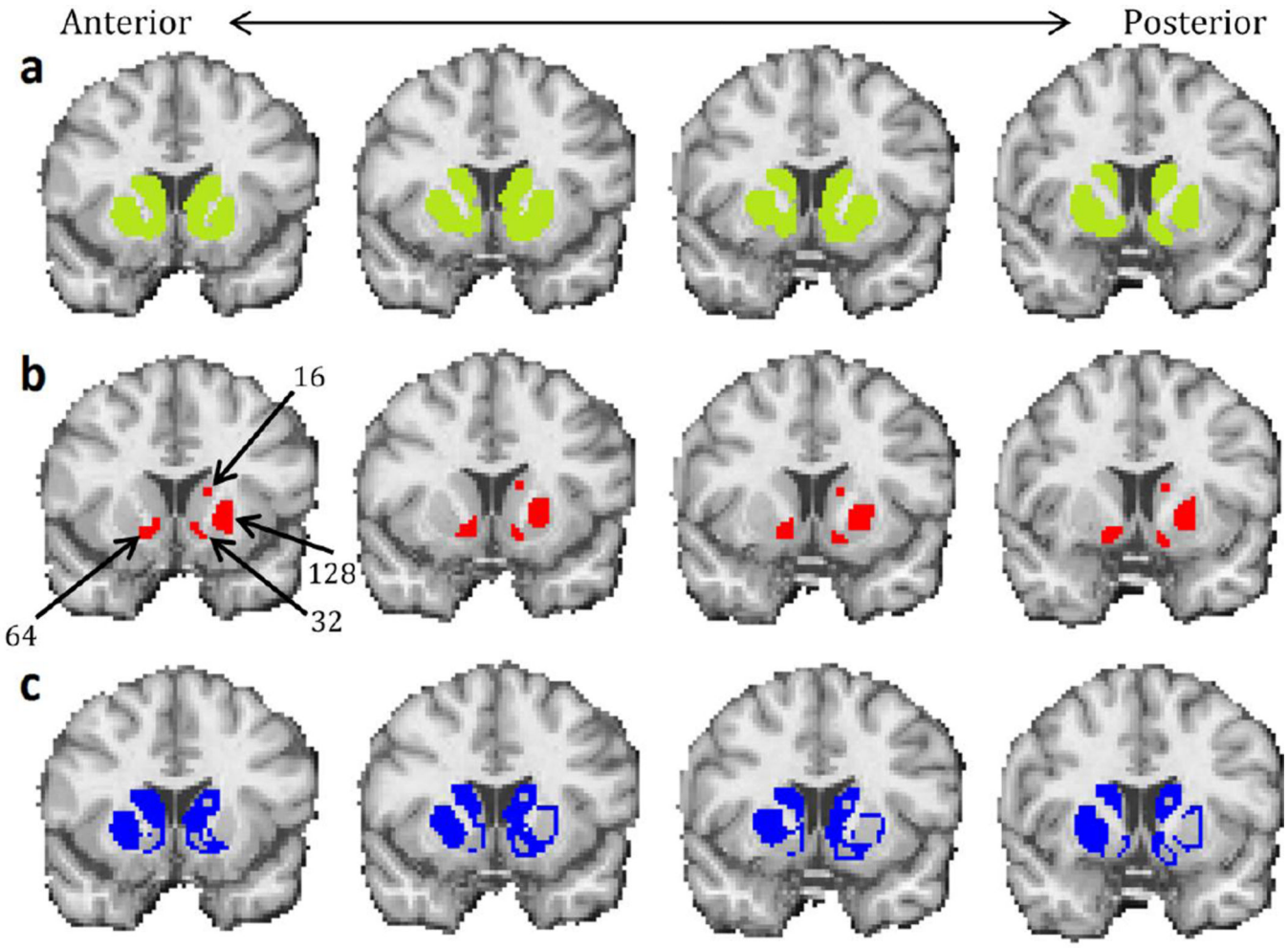

Figure 4.

a. The 4-slice template for precommissural striatum(ventral striatum, dorsal caudate, and dorsal putamen). **b.** The 4 clusters of different sizes where simulated TACs containing DA activation were placed. Number with arrow indicates the number of voxels contained in each cluster. Voxel size is $2 \times 2 \times 2$ mm^3. **c.** Background voxels in the remaining area of the 4-slice striatum template where simulated TACs of the null data were placed.

Author Manuscript Author Manuscript Author Manuscript Author Manuscript

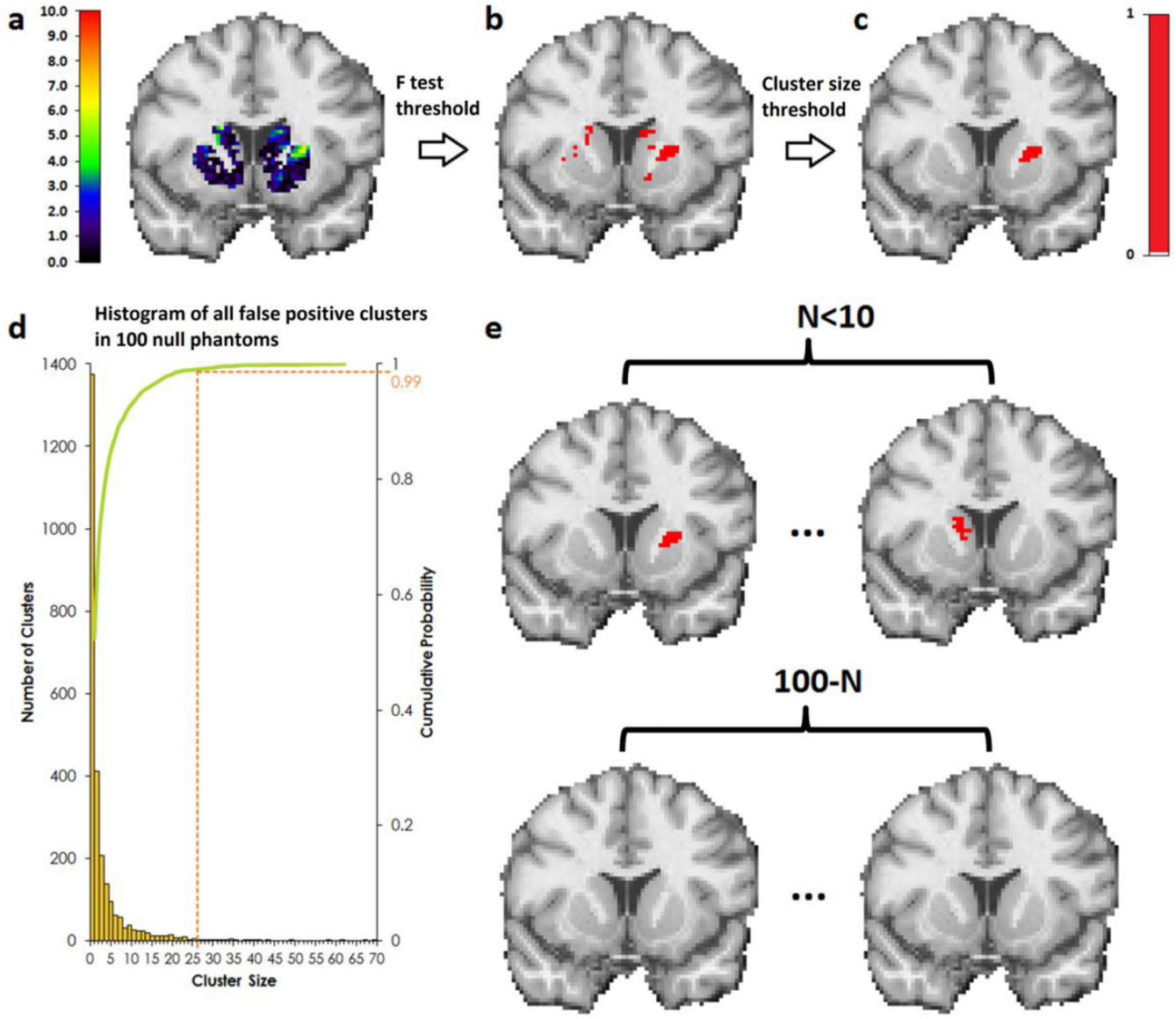

Figure 5.

Processing steps to determine cluster size threshold that corrects for multiple comparisons and controls the false positive rate to be less than 10%. **a.** The F statistics map generated from a null phantom. **b.** The Preliminary Significance Mask thresholded by the F statistics value that translates to a p-value<0.05. **c.** The Final Significance Mask thresholded by the cluster size threshold that corrects for multiple comparisons and controls the false positive rate to be less than 10%. **d.** The histogram of all false positive clusters in the 100 Preliminary Significance Masks generated from 100 simulated null phantoms. A first-pass cluster size threshold was determined so that 99% of the false positive clusters in the 100 Preliminary Significance Masks were eliminated. **e.** The cluster size threshold was further adjusted to ensure that 90 out of 100 Final Significance Masks from simulated null phantoms were completely free of false positive clusters.

Author Manuscript Author Manuscript Author Manuscript Author Manuscript

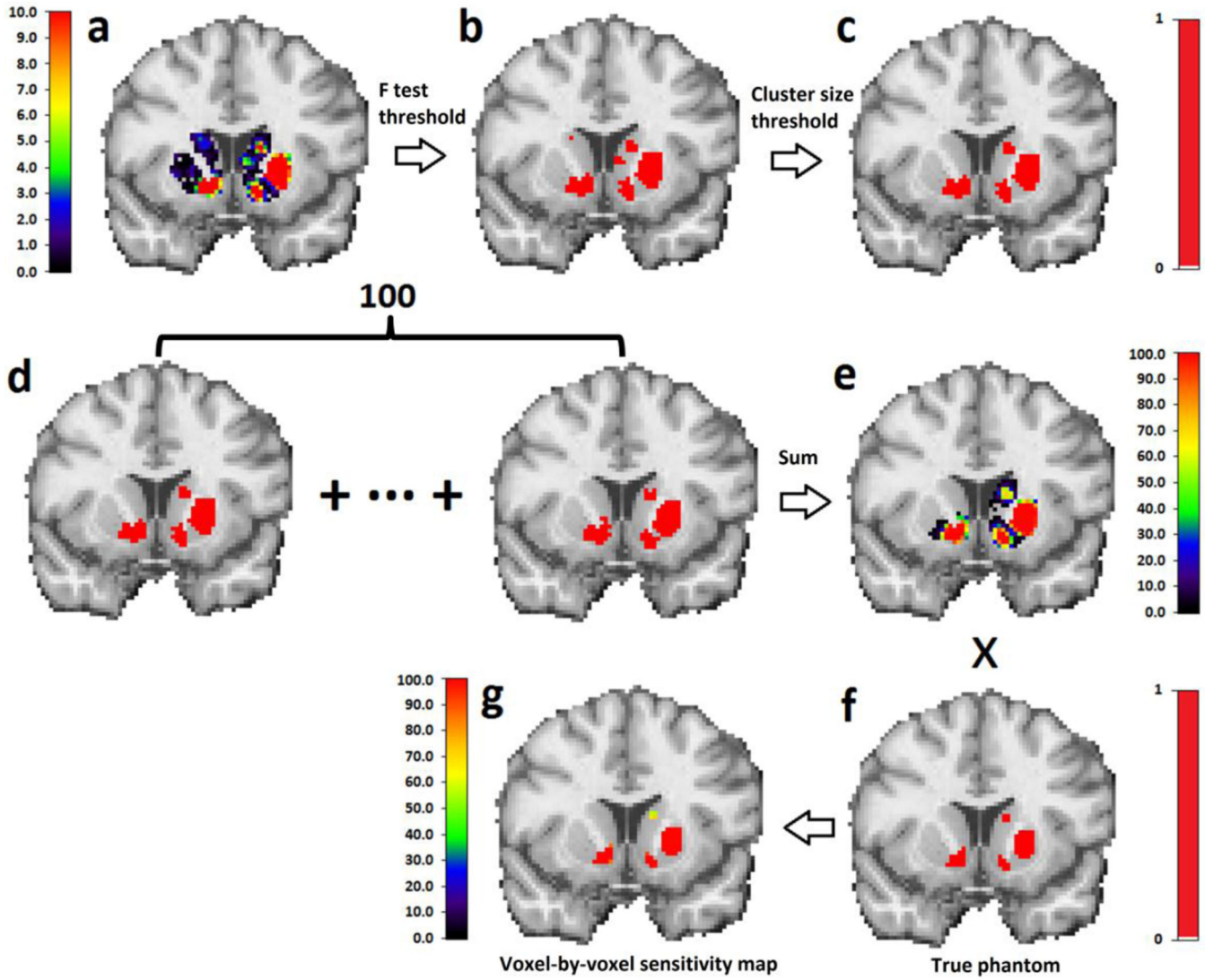

Figure 6.

Processing steps to create a voxel-by-voxel sensitivity map. **a.** The F statistics map generated from a smoking phantom. **b.** The Preliminary Significance Mask thresholded by the F statistics value that translates to a p-value<0.05. **c.** The Final Significance Mask thresholded by the cluster size threshold that corrects for multiple comparisons and controls the false positive rate to be less than 10%. **d.** 100 Final Significance Masks generated from 100 simulated smoking phantoms corresponding to the same study paradigm. **e.** Sum of the 100 Final Significance Masks. **f.** The template of true clusters of activation. **g.** The voxel-by-voxel sensitivity map.

Author Manuscript Author Manuscript Author Manuscript Author Manuscript

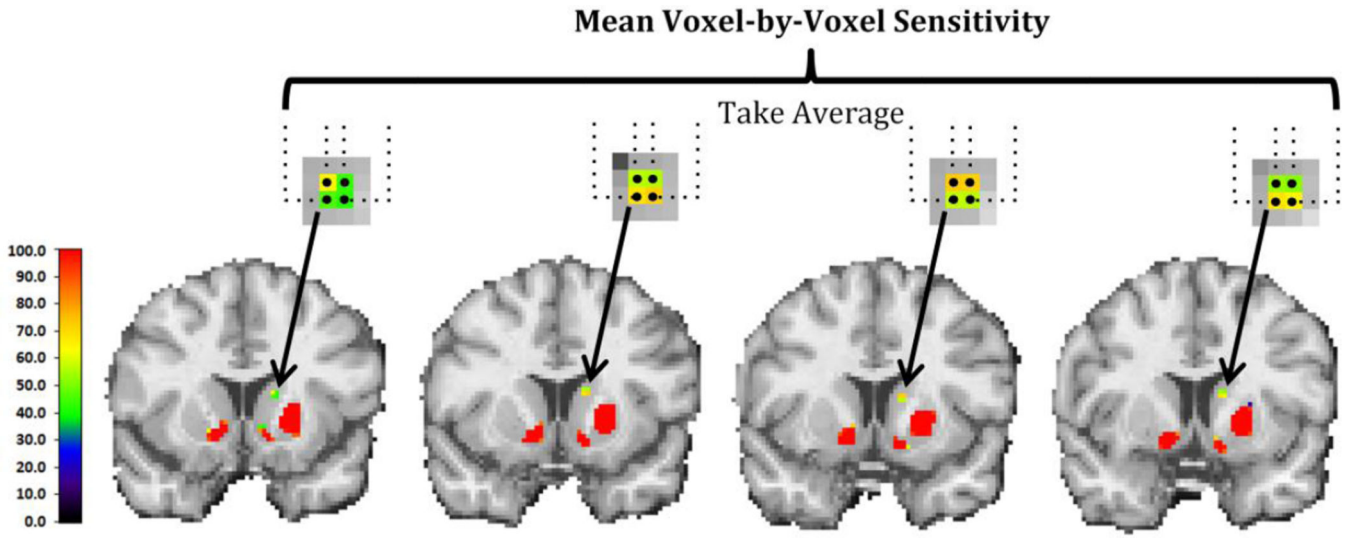

Figure 7.

Calculation of Mean Voxel-by-Voxel (MV) Sensitivity. The MV Sensitivity for a true cluster of activation was calculated as the mean of the voxel-by-voxel sensitivity values across all voxels in that cluster.

Author Manuscript Author Manuscript Author Manuscript Author Manuscript

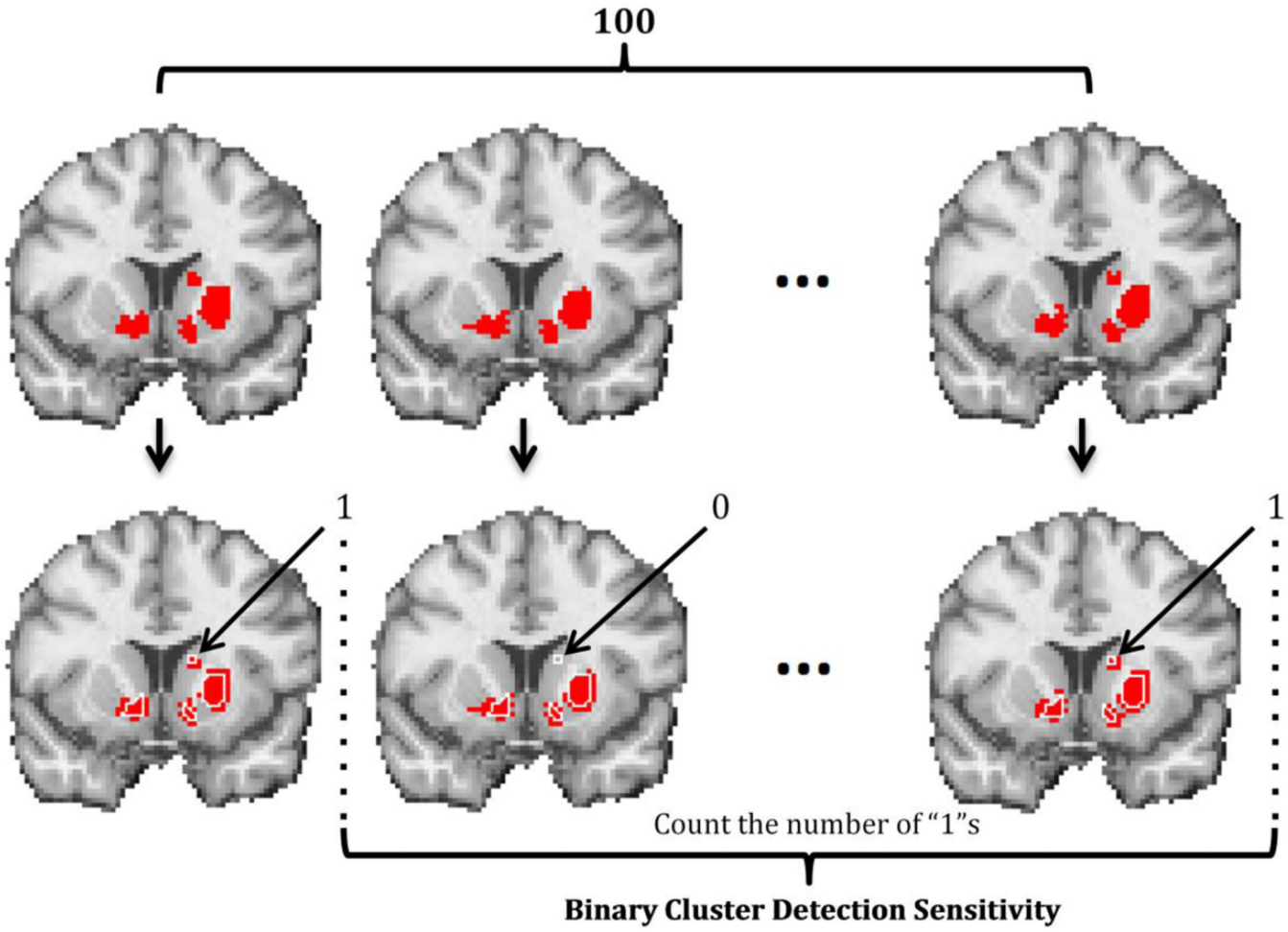

Figure 8.

Calculation of Binary Cluster Detection (BC) Sensitivity. The BC Sensitivity asked the "yes" or "no" question: was a given cluster of activation detected in a simulated phantom. The answer was "yes" (label as "1") when as long as part of the cluster in the true phantom was identified to contain DA release in the simulated phantom. The BC Sensitivity counted the number of simulated phantoms that were positively detected (the number of "1"s) out of 100 simulated phantoms.

Author Manuscript Author Manuscript Author Manuscript Author Manuscript

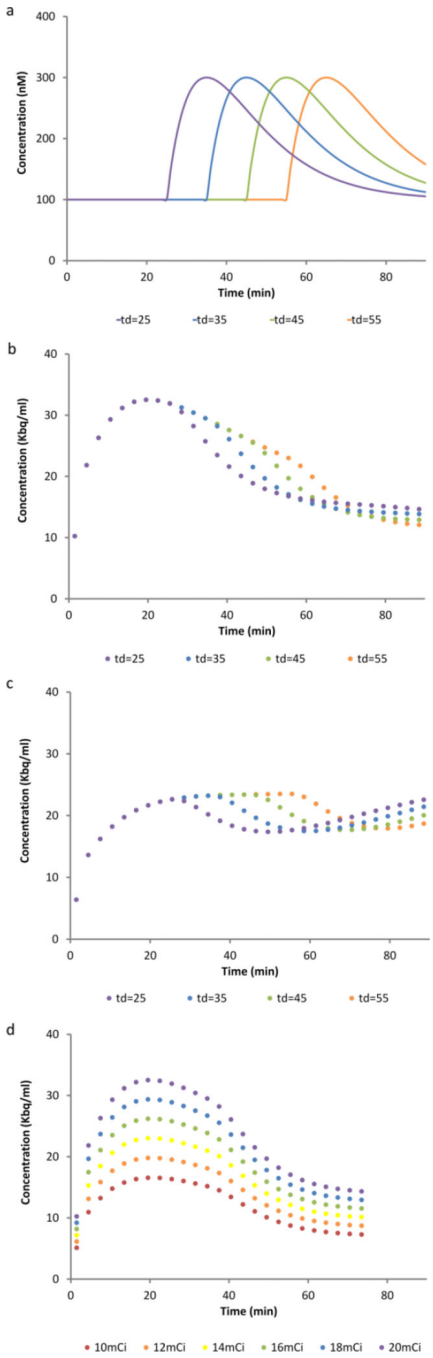

Figure 9.

a. Simulated DA curves with 4 different takeoff times (t_D=[25, 35, 45, 55]min, t_P=t_D+10min) **b.** Simulated noiseless striatal data containing DA activation for 20mCi Bolus studies with a 90min scan duration **c.** Simulated noiseless striatal data containing DA activation for 20mCi B/I studies with a 90min scan duration **d.** Simulated noiseless striatal data containing DA activation that takes off at 35min in 75min Bolus studies with different radioactivity doses.

Author Manuscript Author Manuscript Author Manuscript Author Manuscript

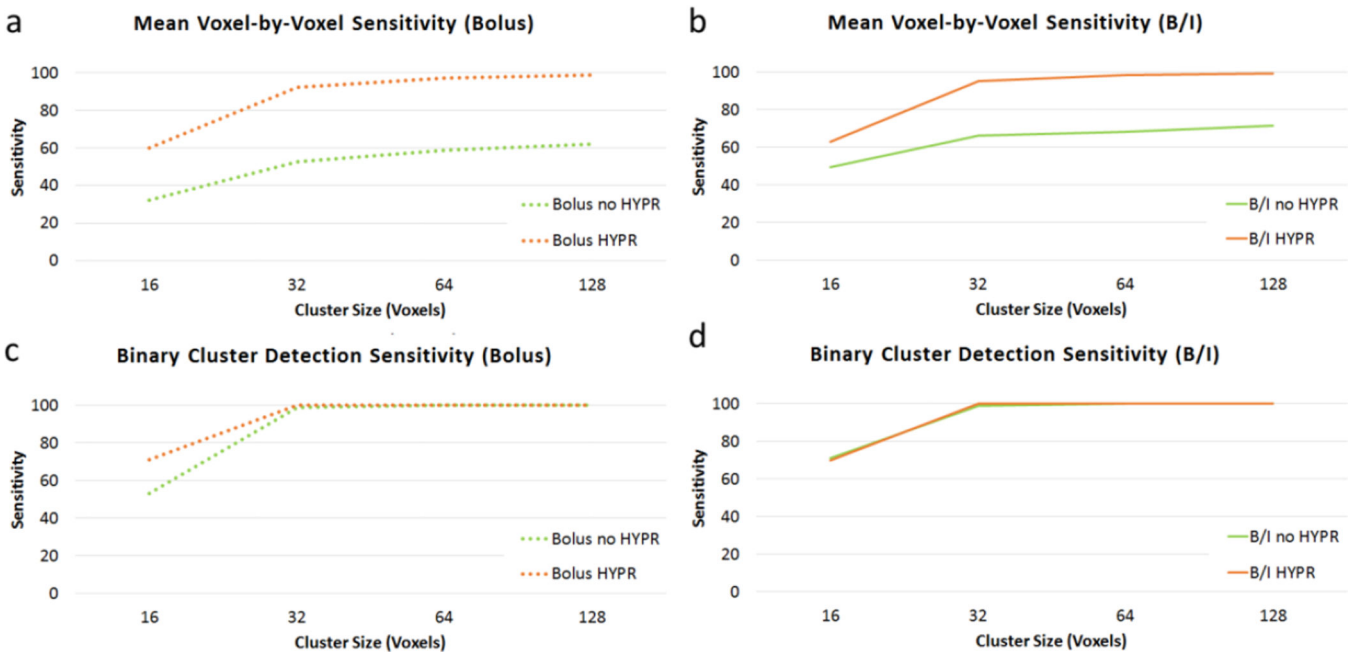

Figure 10.

Metrics of sensitivities for Bolus (**a, c**: dotted lines) and Bolus plus constant infusion (B/I) (**b, d**: solid lines) without (green lines) and with HYPR processing (orange lines).

Author Manuscript Author Manuscript Author Manuscript Author Manuscript

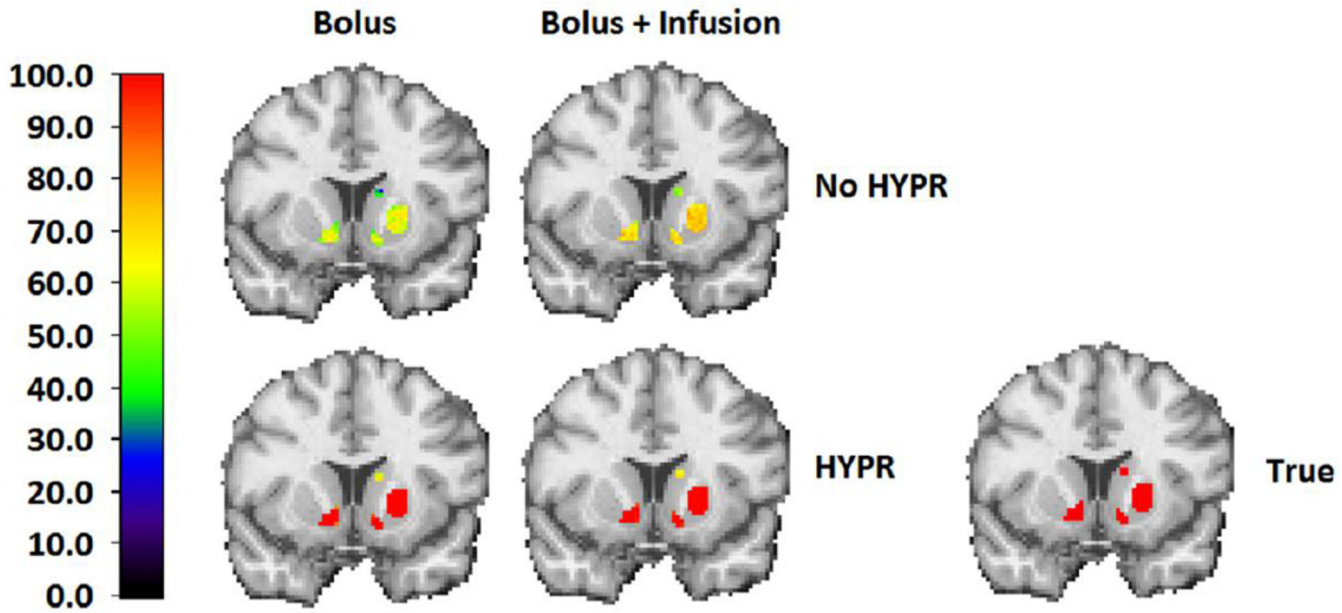

Figure 11.

The voxel-by-voxel sensitivity maps in Bolus and B/I studies without and with HYPR processing. Value in each voxel represents the number of phantoms out of 100 noisy simulated phantoms the same voxel was detected to contain significant DA release.

Author Manuscript Author Manuscript Author Manuscript Author Manuscript

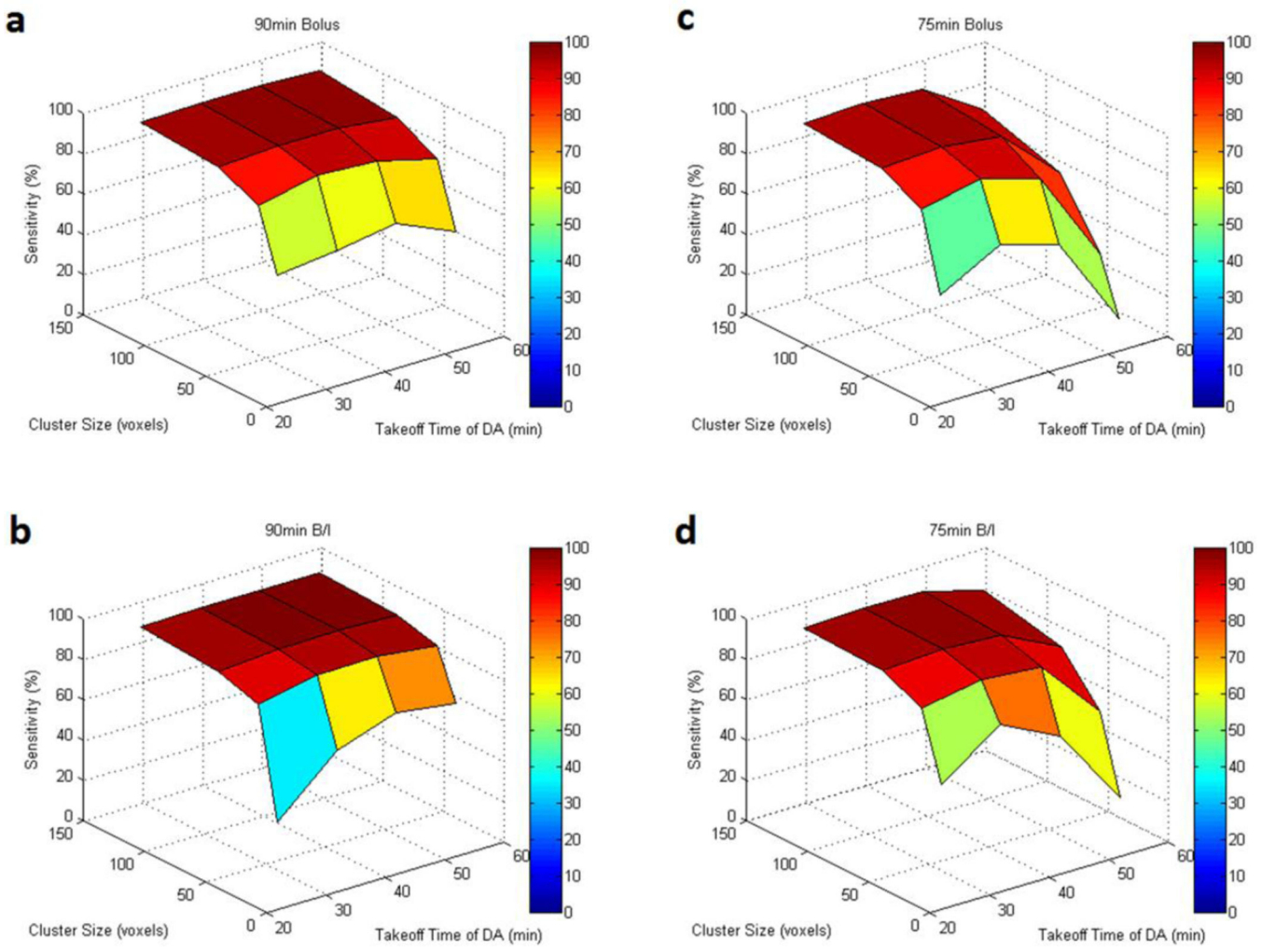

Figure 12.

Mean voxel-by-voxel sensitivity in studies with different takeoff times of DA (t_D=[25, 35, 45, 55]min) for 4 different paradigms: **a.** 90min Bolus study, **b.** 90min B/I study, **c.** 75min Bolus study and **d.** 75min B/I study.

Author Manuscript

Author Manuscript

Author Manuscript

Author Manuscript

Table I

Mean Voxel-by-Voxel Sensitivity in 90min Bolus Studies with Different Takeoff Times of DA

	Cluster size in phantom (voxels)			
Study Paradigm	16	32	64	128
Bolus HYPR t_D=25	56.6%	85.9%	95.7%	97.8%
Bolus HYPR t_D=35	60.0%	92.4%	97.4%	98.8%
Bolus HYPR t_D=45	64.6%	90.7%	97.2%	98.8%
Bolus HYPR t_D=55	51.7%	82.7%	93.5%	97.2%

Author Manuscript

Author Manuscript

Author Manuscript

Author Manuscript

Table II

Binary Cluster Detection Sensitivity in 90min Bolus Studies with Different Takeoff Times of DA

	Cluster size in phantom (voxels)			
Study Paradigm	16	32	64	128
Bolus HYPR t_D=25	68%	99%	100%	100%
Bolus HYPR t_D=35	71%	100%	100%	100%
Bolus HYPR t_D=45	77%	100%	100%	100%
Bolus HYPR t_D=55	76%	100%	100%	100%

Author Manuscript

Author Manuscript

Author Manuscript

Author Manuscript

Table III

Mean Voxel-by-Voxel Sensitivity in 90min B/I Studies with Different Takeoff Times of DA

	Cluster size in phantom (voxels)			
Study Paradigm	16	32	64	128
B/I HYPR t_D=25	35.8%	89.6%	95.8%	98.4%
B/I HYPR t_D=35	62.9%	95.3%	98.6%	99.2%
B/I HYPR t_D=45	72.8%	95.6%	98.9%	99.4%
B/I HYPR t_D=55	68.6%	92.3%	97.8%	98.9%

Author Manuscript

Author Manuscript

Author Manuscript

Author Manuscript

Table IV

Binary Cluster Detection Sensitivity in 90min B/I Studies with Different Takeoff Times of DA

	Cluster size in phantom (voxels)			
Study Paradigm	16	32	64	128
B/I HYPR t_D=25	43%	99%	100%	100%
B/I HYPR t_D=35	70%	100%	100%	100%
B/I HYPR t_D=45	81%	100%	100%	100%
B/I HYPR t_D=55	84%	100%	100%	100%

Author Manuscript

Author Manuscript

Author Manuscript

Author Manuscript

Table V

Mean Voxel-by-Voxel Sensitivity in 75min Bolus Studies with Different Takeoff Times of DA

	Cluster size in phantom (voxels)			
Study Paradigm	16	32	64	128
Bolus HYPR t_D=25	46.3%	84.4%	94.8%	97.6%
Bolus HYPR t_D=35	62.5%	90.8%	96.5%	98.6%
Bolus HYPR t_D=45	53.8%	81.7%	93.1%	97.0%
Bolus HYPR t_D=55	8.3%	35.8%	65.9%	78.0%

Author Manuscript

Author Manuscript

Author Manuscript

Author Manuscript

Table VI

Binary Cluster Detection Sensitivity in 75min Bolus Studies with Different Takeoff Times of DA

	Cluster size in phantom (voxels)			
Study Paradigm	16	32	64	128
Bolus HYPR t_D=25	62%	99%	100%	100%
Bolus HYPR t_D=35	81%	100%	100%	100%
Bolus HYPR t_D=45	80%	100%	100%	100%
Bolus HYPR t_D=55	22%	77%	100%	100%

Author Manuscript

Author Manuscript

Author Manuscript

Author Manuscript

Table VII

Mean Voxel-by-Voxel Sensitivity in 75min B/I Studies with Different Takeoff Times of DA

	Cluster size in phantom (voxels)			
Study Paradigm	16	32	64	128
B/I HYPR t_D=25	54.6%	87.8%	96.4%	98.2%
B/I HYPR t_D=35	75.8%	92.9%	98.3%	99.2%
B/I HYPR t_D=45	60.9%	90.6%	96.8%	98.8%
B/I HYPR t_D=55	21.9%	59.8%	82.1%	90.1%

Author Manuscript

Author Manuscript

Author Manuscript

Author Manuscript

Table VIII

Binary Cluster Detection Sensitivity in 75min B/I Studies with Different Takeoff Times of DA

	Cluster size in phantom (voxels)			
Study Paradigm	16	32	64	128
B/I HYPR t_D=25	68%	100%	100%	100%
B/I HYPR t_D=35	86%	100%	100%	100%
B/I HYPR t_D=45	78%	100%	100%	100%
B/I HYPR t_D=55	39%	94%	100%	100%